Open
ORIGINAL ARTICLE

Cell Research (2015) 25:946-962.
www.nature.com/cr

Mutation of *kri1l* causes definitive hematopoiesis failure via PERK-dependent excessive autophagy induction

Xiao-E Jia[1, 4, *], Ke Ma[1, *], Tao Xu[1, *], Lei Gao[1], Shuang Wu[1], Cong Fu[1], Wenjuan Zhang[1], Zhizhang Wang[1], Kaiyu Liu[6], Mei Dong[1], Changbin Jing[1], Chunguang Ren[1], Zhiwei Dong[1], Yi Chen[2], Yi Jin[2], Qiuhua Huang[2], Xing Chang[1, 9], Min Deng[1], Li Li[8], Lingfei Luo[8], Jun Zhu[7, 9], Yongjun Dang[6], Hung-Chun Chang[5], Leonard I Zon[3], Yi Zhou[3], Saijuan Chen[2, 9], Weijun Pan[1, 9]

[1]Key Laboratory of Stem Cell Biology, Institute of Health Sciences, Shanghai Institutes for Biological Sciences, Chinese Academy of Sciences & Shanghai Jiao Tong University School of Medicine, Shanghai, China; [2]State Key Laboratory for Medical Genomics, Shanghai Institute of Hematology, RuiJin Hospital, Shanghai Jiao Tong University School of Medicine, Shanghai, China; [3]Stem Cell Program, Hematology/Oncology Program at Children's Hospital Boston, Harvard Medical School, Boston, MA 02114, USA; [4]Biomedical Research Center, Baotou Medical College, Baotou, Inner Mongolia Autonomous Region, China; [5]Institute of Neuroscience, Shanghai Institutes for Biological Sciences, Chinese Academy of Sciences, Shanghai, China; [6]Key Laboratory of Metabolism and Molecular Medicine, Ministry of Education, Department of Biochemistry and Molecular Biology, School of Basic Medical Sciences, Fudan University, Shanghai, China; [7]CNRS LIA, Shanghai Institute of Hematology, RuiJin Hospital, 197 RuiJin Road II, Shanghai, China; [8]Key Laboratory of Freshwater Fish Reproduction and Development, Ministry of Education, Laboratory of Molecular Developmental Biology, School of Life Sciences, Southwest University, Beibei, Chongqing, China; [9]Collaborative Innovation Center of Systems Biomedicine, Shanghai Jiao Tong University School of Medicine, Shanghai, China

Dysregulation of ribosome biogenesis causes human diseases, such as Diamond-Blackfan anemia, del (5q-) syndrome and bone marrow failure. However, the mechanisms of blood disorders in these diseases remain elusive. Through genetic mapping, molecular cloning and mechanism characterization of the zebrafish mutant *cas002*, we reveal a novel connection between ribosomal dysfunction and excessive autophagy in the regulation of hematopoietic stem/progenitor cells (HSPCs). *cas002* carries a recessive lethal mutation in *kri1l* gene that encodes an essential component of rRNA small subunit processome. We show that Kri1l is required for normal ribosome biogenesis, expansion of definitive HSPCs and subsequent lineage differentiation. Through live imaging and biochemical studies, we find that loss of Kri1l causes the accumulation of misfolded proteins and excessive PERK activation-dependent autophagy in HSPCs. Blocking autophagy but not inhibiting apoptosis by Bcl2 overexpression can fully rescue hematopoietic defects, but not the lethality of *kri1l*^{cas002} embryos. Treatment with autophagy inhibitors (3-MA and Baf A1) or PERK inhibitor (GSK2656157), or knockdown of *beclin1* or *perk* can markedly restore HSPC proliferation and definitive hematopoietic cell differentiation. These results may provide leads for effective therapeutics that benefit patients with anemia or bone marrow failure caused by ribosome disorders.

***Keywords*:** Hematopoietic stem cells; zebrafish; *kri1l*; ribosome biogenesis; autophagy; PERK; misfolded/unfolded protein
Cell Research (2015) **25**:946-962. doi:10.1038/cr.2015.81; published online 3 July 2015

Introduction

Vertebrate hematopoiesis is an evolutionarily conserved and highly regulated process involving the production of differentiated blood cell lineages from hematopoietic stem cells (HSCs) [1-3]. The zebrafish (*Danio rerio*) is a powerful genetic and developmental model to study the development of vertebrate circulatory system,

*These three authors contributed equally to this work.
Correspondence: Weijun Pan[a], Saijuan Chen[b], Yi Zhou[c]
[a]E-mail: weijunpan@sibs.ac.cn
[b]E-mail: sjchen@stn.sh.cn
[c]E-mail: yzhou@enders.tch.harvard.edu
Received 12 January 2015; revised 3 May 2015; accepted 28 May 2015; published online 3 July 2015

especially hematopoiesis [4, 5]. Definitive hematopoiesis in zebrafish is highly conserved with mammals [6]. It occurs at the ventral wall of dorsal aorta in a structure called aorta-gonad-mesonephros (AGM) around 28 hour post-fertilization (hpf) [7]. By 2 days post-fertilization (dpf), the AGM-derived HSCs migrate to caudal hematopoietic tissue (CHT), an embryonic structure analogous to the mammalian fetal liver [8-10], for rapid pool expansion and lineage differentiation.

Normal ribosome biogenesis is critical for cell survival, proliferation and function. In eukaryotic cells the small subunit (SSU) processome, a ribonucleoprotein complex, plays essential roles in 18S rRNA maturation, small ribosomal subunit assembly and subsequent ribosome biogenesis [11]. The SSU processome is composed of pre-rRNA, small nucleolar RNAs and more than 70 different associated proteins. Dysfunction of ribosome biogenesis is associated with human diseases, including Diamond–Blackfan anemia (DBA), 5q minus (del (5q−)) syndrome, dyskeratosis congenita and Bowen-Conradi syndrome [12-14]. In addition to carrying genetic mutations affecting ribosome biogenesis, these human diseases share same clinical features, and are thus termed as "ribosomopathies" [13].

Previous works have shown that upregulation of p53 by ribosome dysfunction contributes to bone marrow failure syndromes [15] that have been genetically mapped to loss-of-function mutations in rps14 [16], rps19 [17, 18], rpl11 [19] and rps29 [15]. The apoptotic phenotype of hematopoietic cells in these diseases can be partially restored by p53 downregulation [16, 17]. However, some studies have reported that p53 pathway is not involved in some ribosome biogenesis disorders [20-22]. Furthermore, not all bone marrow samples from patients with del (5q−) syndrome or DBA show p53 activation, suggesting that other mechanisms may contribute to ribosomopathies [23]. For example, loss of *pwhp2h* causes gut degeneration and hyperactivated autophagy in a p53- and mTOR-independent manner [21]. Knockdown of Rpl22 in zebrafish embryos blocks T-lineage progenitor development, while knockdown of the Rpl22 paralog Rpl22l impairs the emergence of HSC in AGM by abrogating Smad1 expression and Runx1 induction [24].

Autophagy and apoptosis are two major stress-response pathways. Dysregulation of autophagy has been linked to many human diseases such as neurodegeneration [25, 26], autoimmunity and cancer [27, 28]. Multiple upstream signaling mechanisms, including mTOR pathway, unfolded protein response (UPR), ER stress and nutrition stress regulate autophagy, with Beclin1-VPS34 complex playing an important role in autophagy initiation [29, 30]. Autophagy is a critical mechanism that protects HSCs from stress damages [31]. In mice, a conditional deletion of *atg7* in HSCs renders the loss of HSC's self-renewal property and severe myeloproliferation due to a failure of HSPCs to respond normally to stress from reactive oxygen species (ROS) [32]. Appropriate autophagy level is also important for lymphocyte survival [33, 34] and erythroid cell maturation [35-37]. Patients with certain ribosomopathies have elevated levels of autophagy in peripheral blood cells resulted from S6K-induced inhibition on insulin pathway activation [38]. However, the potential cures for these disorders have not been found.

In the present study, we report that *kri1l* gene is essential for definitive hematopoiesis. Loss of Kri1l, a critical component of SSU complex, causes ribosomal biogenesis defects, accumulation of misfolded proteins and activation of PERK-eif2a signaling. These deficiencies subsequently hyperactivate autophagy and ultimately lead to the inhibition of HSPC proliferation. Treatment with autophagy or PERK inhibitors, or knockdown of *beclin1* or *perk* by morpholino (MO), can successfully rescue HSPC proliferation and lineage differentiation in *kri1l* mutant.

Results

cas002 mutant displays a hematopoietic failure phenotype

In a large-scale ENU mutagenesis screen for definitive hematopoietic mutations, we obtained *cas002*, a novel mutant with severe hematopoietic defects and recessive lethality. *cas002* embryos are morphologically indistinguishable from wild-type siblings before 3 dpf, with normal blood flow and heart beats (Figure 1A-1B). However, whole-mount *in situ* hybridization (WISH) of *cmyb* reveals a markedly reduced HSPC population in caudal hematopoietic tissue (CHT) of mutant embryos at 3 dpf (Figure 1C-1D), and in CHT, thymus and kidney at 5 dpf (Figure 1E-1F). *cas002* mutant embryos eventually die at 6-10 dpf with abnormal head shape, cardiac edema and smaller eyes.

To examine hematopoiesis phenotype in detail, we performed WISH analysis of different cell lineage markers: *gata1* (erythrocyte progenitors), *αe1-globin* (embryonic erythrocytes), *l-plastin* (pan-myeloid cells), *lyz* and *mpo* (neutrophils). The expression of these markers is the same as wild-type siblings at 3 dpf (Supplementary information, Figure S1), but becomes significantly reduced in *cas002* mutant embryos at 5 dpf (Supplementary information, Figure S2A-S2J). The expression of *rag1* (T lymphocyte), is substantially reduced at 4 dpf in *cas002* (Supplementary information, Figure S2K-S2L),

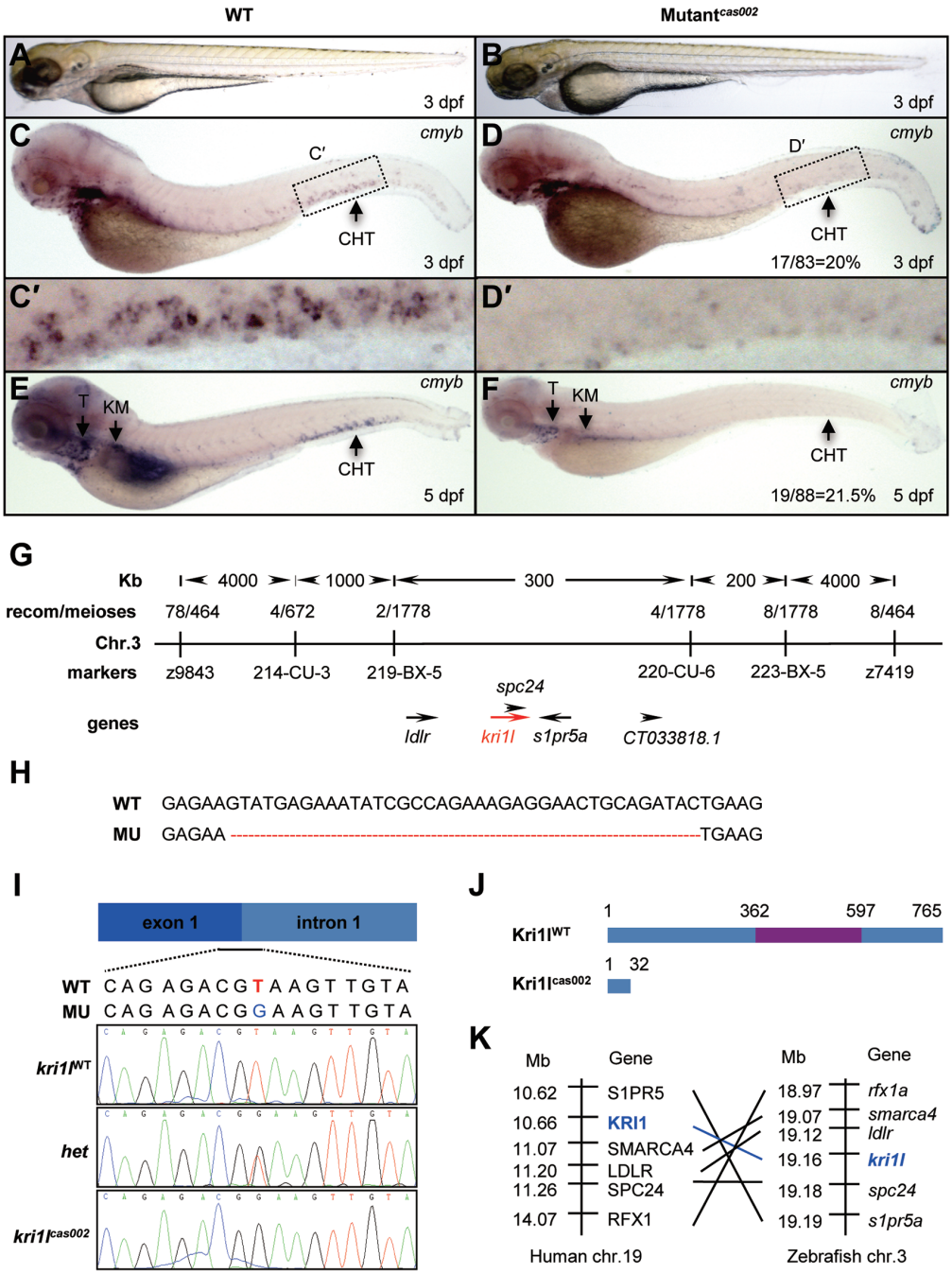

Figure 1 Hematopoietic defects and positional cloning of *cas002* mutant. **(A-B)** Light microscope images of zebrafish wild-type (WT) and *cas002* embryos at 3 dpf. **(C-F)** WISH analysis of *cmyb* expression in WT and *cas002* embryos at indicated development stages. Black arrows indicate thymus, kidney marrow and CHT. **(C′-D′)** enlarged CHT regions in **C** and **D**. **(G)** Genetic mapping of the *cas002* region on chromosome 3. Bulk segregation analysis locates *cas002* mutation to Chr. 3. Fine mapping using SSLPs narrows down to a region between markers 219-BX-5 and 220-CU-6, containing *kri1l* and four other genes as indicated. **(H)** The sequencing results of *kri1l* cDNA from mutant embryos show a 38 bp deletion (MU) compared with *kri1l* cDNA from WT embryos. **(I, J)** The sequencing result of *kri1l* genomic DNA shows a T-G transversion at the *kri1l* exon 1-intron 1 consensus splicing donor site **(I)**, which causes a frame shift **(H)** and a premature stop codon leading to the production of a truncated Kri1l protein **(J)**. **(K)** Synteny between zebrafish *kri1l I* and human *KRI1* loci. (Left) Six genes, including *KRI1*, are located within a genomic region on human chromosome 19. (Right) Six zebrafish homologs are listed according to their map positions on chromosome 3 (Ensembl website). CHT, caudal hematopoietic tissue; KM, kidney marrow; Mb, mega base; T, thymus; het, heterozygote.

indicating that lymphoid development is also impaired. In contrast, primitive hematopoiesis and vascular morphogenesis are intact in *cas002* embryos (Supplementary information, Figure S3). To identify the onset of hematopoiesis failure in *cas002* mutant embryos, we traced expression of *cmyb* and *runx1*, another HSC marker, at earlier developmental time points (Supplementary information, Figure S4). Both *cmyb* and *runx1* are expressed normally in the AGM from 36 hpf to 40 hpf (Supplementary information, Figures S4A-S4D and S4C′-S4D′) and at 36 hpf (Supplementary information, Figure S5A-S5B), respectively, suggesting a normal hematopoiesis in the AGM at these stages. A marginal decrease of *cmyb* expression is detectable in the CHT region at 40 hpf (Supplementary information, Figure S4C″-S4D″). By 4 dpf, the expression of *cmyb* is almost undetectable in the CHT, kidney and thymus of *cas002* mutant embryos (Supplementary information, Figure S4K-S4L). Another HSPC marker *scl* is also markedly reduced from 3 dpf (Supplementary information, Figure S5C-S5H). In addition, *cas002* mutant embryos have significantly fewer $EGFP^+$ cells (marked by eGFP under *cmyb* promoter) than the wild type (Supplementary information, Figure S6A-S6G). Taken together, these results suggest that definitive HSPCs in the CHT are severely disrupted in *cas002* mutant embryos.

cas002 mutant carries a defective kri1l gene

To understand the mechanism of hematopoietic failure in *cas002* mutant, we carried out positional cloning [39]. The mutation was first mapped on chromosome 3 by bulk segregation analysis (BSA). Simple sequence length polymorphism (SSLP)-based fine mapping established that the mutation lies within a 300 kb region between two markers: 219-BX-5 and 220-CU-6 (Figure 1G). We sequenced all five candidate genes in this region, and found a 38 bp deletion in *kri1l* cDNA in *cas002* mutant (Figure 1H). Genomic DNA sequencing of *kri1l* gene revealed that a consensus splicing donor site at the boundary between exon1 and intron1 is disrupted by a T-to-G transversion in *cas002* mutant (Figure 1I). This mutation yields an abnormally spliced transcript with a frame shift and a premature stop codon in exon2. The altered transcript is predicted to encode a highly truncated Kri1l peptide 32 amino acid in length (Figure 1J). This point mutation is not found among five commonly used laboratory zebrafish strains (Tu, AB, WIK, Longfin and Shanghai; Supplementary information, Figure S6H), excluding the possibility of single-nucleotide polymorphism [40]. The zebrafish *kri1l* gene is 62% identical with the human *KRI1*. The *kri1l* locus on zebrafish chromosome 3 is syntenic to a region of human chromosome 19 that contains the *KRI1* gene, based on the conserved locations of neighboring orthologous gene pairs (*S1PR5*, *SMARCA4* and *LDLR*; Figure 1K). These findings suggest that zebrafish *kri1l* gene is an ortholog of human *KRI1*.

Mutated kri1l causes cas002 phenotypes

To confirm that the mutation in *kri1l* gene is responsible for *cas002* phenotypes, we microinjected *kri1l* ATG morpholino (MO) and splicing MO to suppress translation and maturation of *kri1l* mRNA, respectively, into wild-type zebrafish embryos. A construct containing a 60-bp fragment including *kri1l* ATG MO-binding site fused to the N-terminus of EGFP (Supplementary information, Figure S7E) was co-injected with *kri1l* ATG MO; the expression of EGFP was successfully blocked (Supplementary information, Figure S7A-S7D). The *kri1l* splicing MO caused splicing defect in the endogenous *kri1l* transcripts (Supplementary information, Figure S7F). *cmyb* expression and $EGFP^+$ cell numbers in both morphants in Tg (*cmyb:egfp*) background were significantly reduced, indicating that *kri1l* knockdown reproduces hematopoietic defects found in *cas002* mutant (Figure 2A-2C and Supplementary information, Figure S7G-S7H).

To provide further evidence that *kri1l* is defective in *cas002* mutant, we performed a rescue experiment by microinjection of synthetic wild-type *kri1l* mRNA into *cas002* mutant embryos. As monitored by WISH analysis of *cmyb* expression, we found that the definitive hematopoiesis was fully rescued by wild-type Kri1l overexpression (Figure 2D-2F). In summary, results from positional cloning, MO phenocopy and mRNA rescue experiments strongly suggest that the T-to-G mutation in zebrafish *kri1l* gene is responsible for the defective hematopoiesis in *cas002* mutant embryos. We thus rename the mutant as $kri1l^{cas002}$.

To understand the role of *kri1l* in embryogenesis, especially in definitive hematopoiesis, we examined the temporal and spatial expression of *kri1l* by WISH analysis. The *kri1l* transcript is expressed as maternal mRNA. During early development, *kri1l* is expressed ubiquitously throughout the embryo and enriched in somites at 18 hpf and eyes at 22 hpf (Supplementary information, Figure S8).

In yeast, KRI1 is a component of the SSU complex, and plays an essential role in 40S ribosome subunit formation and ribosomal polysome assembly. Mechanistically, loss of KRI1 results in instability of 18S rRNA precursor and dramatic reduction of mature 18S rRNA [41]. We asked whether $kri1l^{cas002}$ mutant embryos have similar defects in ribosome biogenesis. E-bioanalyser analysis of total RNA revealed a dramatic reduction in

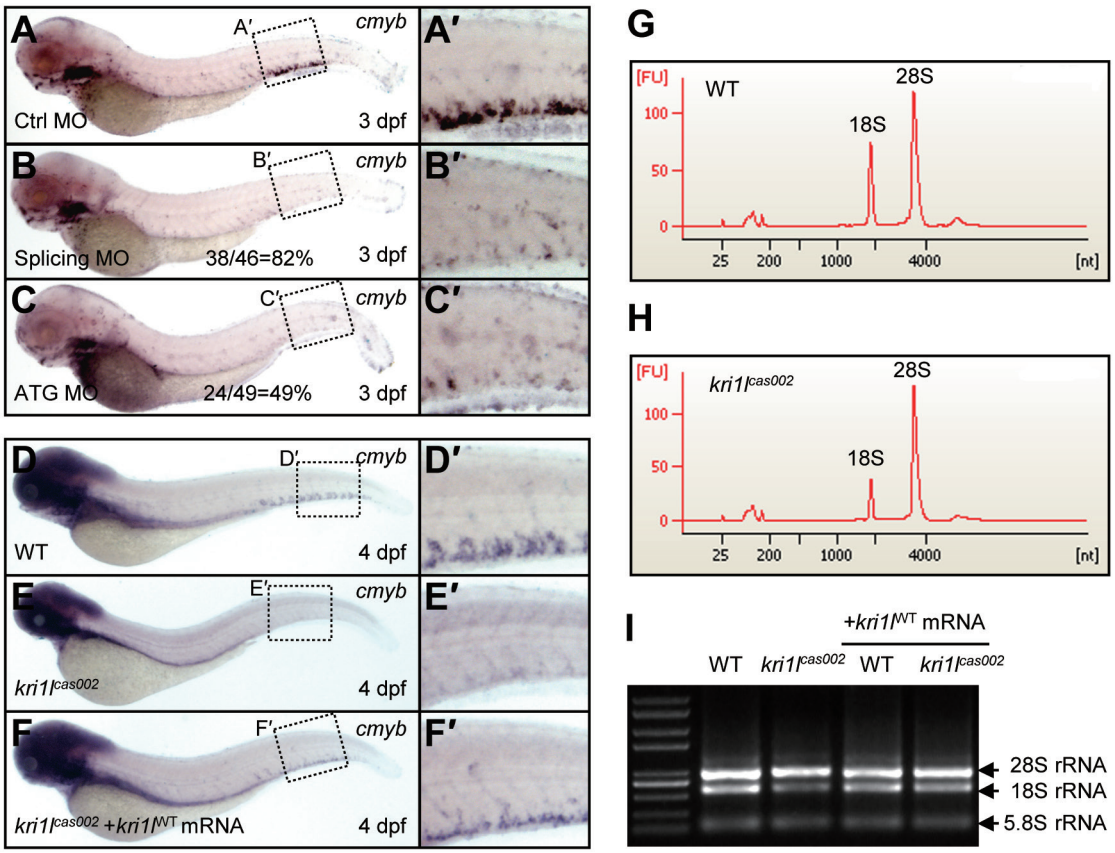

Figure 2 Mutation in *kri1l* gene is responsible for *cas002* phenotypes. **(A-C)** Morpholino knockdown of *kri1l* phenocopies *cas002* mutant. *kri1l* ATG MO and splicing MO were injected into wild-type embryos at one-cell stage. At 3 dpf, the injected embryos were fixed and analyzed for *cmyb* expression by WISH. The percentage of morphants with the reduced *cmyb* expression phenotype is listed at the bottom of **B** and **C**. **(D-F)** Transient expression of wild-type *kri1l* mRNA rescues *cas002* mutant. *cas002* mutant embryos at one-cell stage were injected with synthesized wild type *kri1l* mRNA. The injected embryos were fixed for analysis of *cmyb* gene expression using WISH at 4 dpf. After WISH and photographing, all embryos were genotyped by sequencing of genomic DNA; the percentage of the rescue was then evaluated. The percentage of fully rescued mutant embryos is about 54% (50/92), while the rest are partially rescued. **(A′-F′)** Details of *cmyb* expression in CHT regions in **A-F**. **(G-H)** E-Bioanalyser analysis of total RNA isolated from WT and *kri1l*^{cas002} embryo pools (each pool of 12 embryos) at 3 dpf. A significant reduction in the 18S peak but unchanged 28S peak in *kri1l*^{cas002} results in an elevated 28S/18S rRNA ratio. **(I)** The 18S rRNA reduction can be restored in mutant embryos by injection of *kri1l*^{WT} mRNA.

mature 18S rRNA in *kri1l*^{cas002} embryos, while the amount of 28S rRNA was normal (Figure 2G-2H), which is consistent with previous observations in KRI1-deficient yeast cells. Reduced 18S rRNA could be restored by microinjection of wild-type *kri1l* mRNA into *kri1l*^{cas002} mutants (Figure 2I). We further examined the total protein level by bicinchoninic acid (BCA) protein quantitation and confirmed impaired protein synthesis in *kri1l*^{cas002} mutant embryos (Supplementary information, Figure S9A-S9C) (P = 0.0003). Sequencing of 18S rRNA in wild-type and *kri1l*^{cas002} mutant embryos showed no difference; however, 80S ribosome and polysome formation were impaired in *kri1l*^{cas002} mutant embryos with excessive 60S ribosome subunits (Supplementary information, Figure S9D).

Bcl2 rescues hematopoiesis in kri1l^{cas002} *mutant*

To elucidate the mechanism of defective HSPCs in *kri1l* mutant, we examined HSPC proliferation by calculating the proportion of phospho-histone 3 (pH3) immunostaining-positive cells in total HSPC (*cmyb* WISH positive) during hematopoietic development (Figure 3A, 3F, 3G-3R and Supplementary information, Figure S10). At 40 hpf, the percentage of proliferative HSPCs (pH3$^+$*c-myb*$^+$/*cmyb*$^+$) in *kri1l*^{cas002} mutant embryos was nearly the same as that in wild-type siblings in the AGM (Figure 3A and Supplementary information, Figure S10A-S10H; P = 0.0873), but was significantly reduced in the CHT (Figure 3A and Supplementary information, Figure S10I-S10P; P < 0.0001), and was further decreased in the CHT at 2

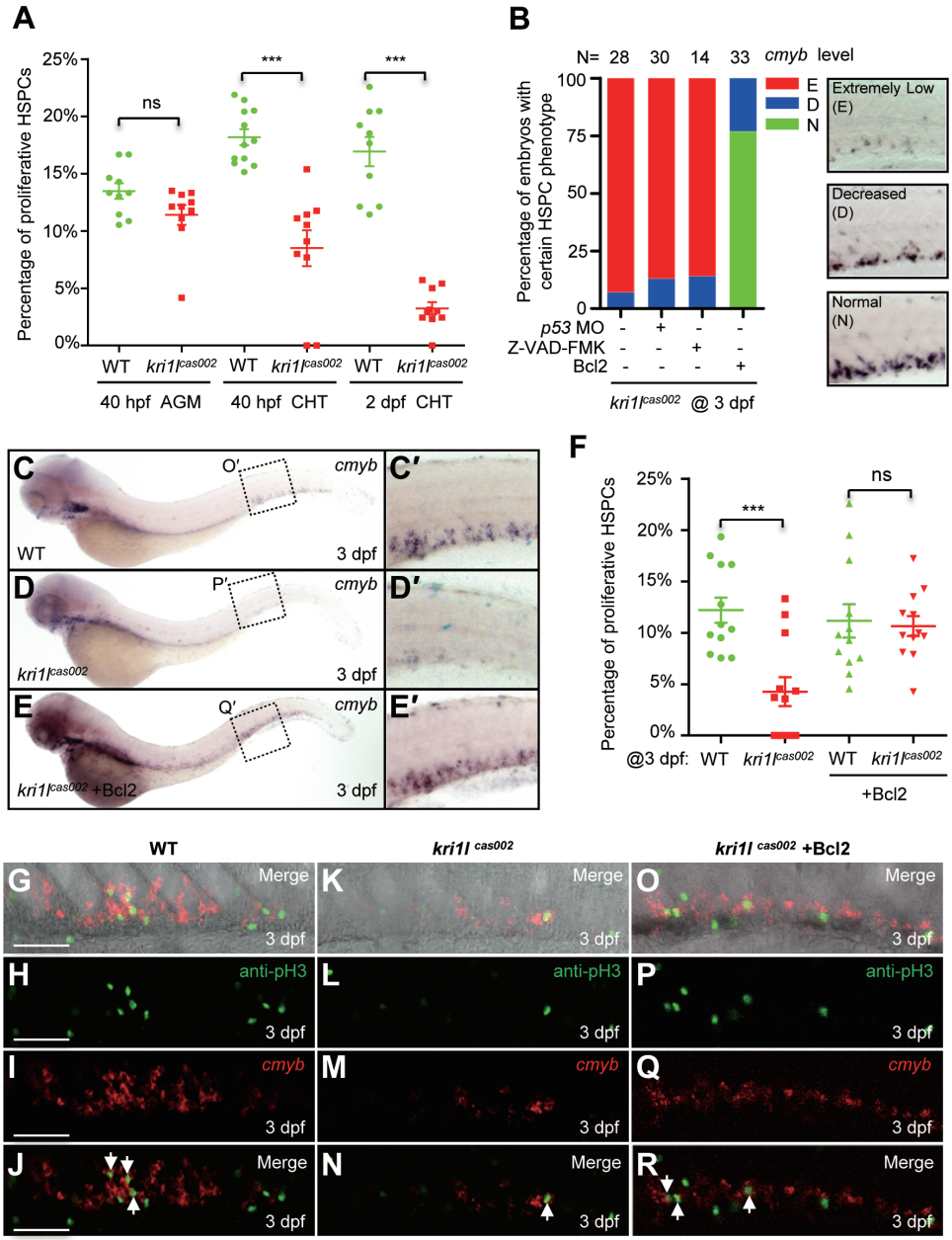

Figure 3 Transient expression of Bcl2 rescues the defective hematopoiesis in *kri1l*^{cas002} mutant embryos. **(A)** Statistic analysis of the proportion of proliferative HSPCs (*cmyb* and PH3 double positive) in total HSPCs in *kri1l*^{cas002} mutant embryos and wild-type siblings during hematopoietic development (40 hpf-2 dpf). N ≥ 10 for each group. 40 hpf AGM, $p = 0.0873$; 40 hpf CHT, $p < 0.0001$; 2 dpf CHT, $p<0.0001$. Error bars represent SEM. $^{**}P \le 0.01$; $^{***}P \le 0.001$ (Student's *t*-test). **(B)** Proportion of *kri1l*^{cas002} mutant embryos with classified hematopoiesis phenotype (indicated by *cmyb* staining) with or without microinjection of *p53* MO, treatment with caspase inhibitor (Z-VAD-FMK) or Bcl2 expression, respectively. **(C-E)** The CHT hematopoiesis is recovered by Bcl2 overexpression in *kri1l*^{cas002} mutant embryos. Embryos from two heterozygous parents were injected with *bcl2* mRNA at one-cell stage and harvested for WISH analysis. After WISH and photographing, all embryos were genotyped by genomic DNA sequencing; percentage of rescue was then calculated. 26 out of 33 mutant embryos injected at one-cell stage with *bcl2* mRNA are fully rescued, while the rest of embryos are partially rescued. **(C′-E′)** The enlarged CHT regions. **(F)** Percentage of the proliferative HSPCs in the CHT of *kri1l*^{cas002} mutant embryos and wild-type siblings with or without Bcl2 overexpression at 3 dpf. $N = 12$ for each group. Without Bcl2 overexpression, $p < 0.0001$; With Bcl2 overexpression, $p = 0.3136$. Error bars represent SEM. $^{**}P \le 0.01$; $^{***}P \le 0.001$ (Student's *t*-test). **(G-R)** Representative confocal images of double staining of *cmyb* RNA (red) and pH3 protein (green) in the CHT at 3 dpf. **G**, **K** and **O** are bright-field images overlaid with fluorescent staining. Scale bars, 50 μm.

dpf (Figure 3A and Supplementary information, Figure S10Q-S10X; $P < 0.0001$) and 3 dpf (Figure 3F-3R) ($P = 0.0003$).

Previous reports have demonstrated that p53-dependent apoptosis pathway is activated and responsible for hematopoietic defects in both ribosomopathy-related mice and zebrafish models [15-18]. We carried out terminal transferase dUTP nick end labeling (TUNEL) assays in wild-type siblings and *kri1l*^{cas002} mutant embryos from 40 hpf to 3 dpf; however, there was no significant difference in apoptotic signals in the CHT region between two genotypes (Supplementary information, Figure S11).

Furthermore, we microinjected *p53* MO [42] into *kri1l*^{cas002} mutant embryos (Figure 3B and Supplementary information, Figure S12A-S12D), and *kri1l* MO into *p53*^{M214K} mutant embryos (Supplementary information, Figure S13A-S13D). The defective hematopoiesis remained in these morphants, suggesting that p53-dependent apoptosis is not responsible for the hematopoietic failure in *kri1l*^{cas002} mutant. We further tested whether the activation of caspase pathway contributes to HSPC defects and found treatment of pan-caspase inhibitor, Z-VAD-FMK peptide, could not rescue *kri1l*^{cas002} phenotype (Figure 3B and Supplementary information, Figure S12E-S12F). Quantitative PCR and immunoblotting analysis also showed that Δ113-p53, an inhibitor of full-length p53 [43], but not full-length p53, was dramatically upregulated in *kri1l*^{cas002} mutant embryos (Supplementary information, Figure S14).

In parallel, we overexpressed an EGFP-Bcl2 fusion protein in *kri1l*^{cas002} mutant embryos. To our surprise, microinjection of *egfp-bcl2* mRNA fully restored *cmyb* expression in the CHT of *kri1l*^{cas002} mutant embryos at 3 dpf (Figure 3B-3E). We performed WISH analysis of *αe1-globin* and *lyz* expression at 4 dpf, and found Bcl2 overexpression also successfully restored the erythrocytes (74%; Supplementary information, Figure S15A-S15D) and neutrophils (61%; Supplementary information, Figure S15E-S15H). Very importantly, ectopic expression of Bcl2 almost fully restored the percentage of proliferating HSPCs (Figure 3F-3R; $P = 0.3136$) in *kri1l*^{cas002} mutant embryos.

Autophagy is hyperactivated in kri1l^{cas002} *mutant*

Recent reports have shown that Bcl2 functions not only as an anti-apoptosis protein, but also as an anti-autophagy protein by interacting with Beclin1 and disrupting VPS34-Beclin1 complex [44, 45]. To check whether the regulatory role of Bcl2 in autophagy is responsible for the rescue of HSPC in *kri1l*^{cas002} mutant, we carried out immunoblotting on the whole embryo lysates using an antibody against an autophagy marker, microtubule-associated protein light chain 3 (Lc3) [46, 47]. We found the level of Lc3-II in *kri1l*^{cas002} mutant was significantly higher than that in wild-type embryos (Figure 4A), and it could not be rescued in *p53*^{M214K} mutant background [48] (Supplementary information, Figure S13E). In addition, we found that the level of p62 protein [49], a well-characterized autophagy substrate, was decreased in *kri1l*^{cas002} mutant embryos, while the level of autophagy initiation factor Beclin1 was unchanged in the mutant embryos (Figure 4A and Supplementary information, Figure S14A).

In order to directly observe the autophagy level in live *kri1l*^{cas002} mutant [46, 50], we injected a *mCherry-lc3* fusion RNA (*in vitro* transcribed from a previously described construct [51]) into wild-type or *kri1l*^{cas002} embryos transgenic for *cmyb*:*egfp* at one-cell stage. At 3 dpf, abundant Lc3-II puncta (indicating autophagosomes) were present in *kri1l*^{cas002} EGFP^{+} cells in the CHT (Figure 4B-4H; $P = 0.004$), and this phenomenon became more obvious after chloroquine treatment, which is known to block the degradation of autophagosome [52, 53] (Figure 4B, 4I-4N; $P = 0.0008$). The increased Lc3-II puncta in HSPC could be found as early as 40 hpf in the CHT of *kri1l*^{cas002} mutant (Supplementary information, Figure S16). Analysis of electron micrographs further confirmed a significant increase of autophagosome-like structures above the wild-type level in the CHT region of *kri1l*^{cas002} mutant (Supplementary information, Figure S17). These results suggest that the autophagy level is significantly elevated in *kri1l*^{cas002} mutant, and this change may correlate with the reduction of HSPCs.

To test whether Bcl2 overexpression rescues the hematopoietic failure in *kri1l*^{cas002} mutant embryo through inhibiting autophagy, we evaluated the Lc3-II level in *kri1l*^{cas002} mutant with or without overexpression of Bcl2. Consistent with our hypothesis, Bcl2 overexpression significantly reduced the Lc3-II level in *kri1l*^{cas002} mutant (Figure 4O). mCherry-Lc3-labeled autophagosomes in EGFP^{+} HSPCs were also markedly decreased in Bcl2-overexpressed *kri1l*^{cas002} mutant (Figure 4P-4S; $P = 0.0021$), suggesting Bcl2 rescues *kri1l*^{cas002} hematopoietic phenotype through its anti-autophagy function.

Inhibition of autophagy restores hematopoiesis in kri1l^{cas002} *mutant*

Autophagy inhibitors have been successfully developed to target different stages of autophagic flux. We hypothesized that the treatment with these inhibitors, or knockdown of the autophagy initiation factor Beclin1, might mimic the effect of Bcl2 overexpression in restoring hematopoiesis in *kri1l*^{cas002} mutant. Indeed, *kri1l*^{cas002} mutant embryos treated with 3-MA [54] at 10 mM or Bafilomycin A1 (Baf A1) [55] at 25 nM for 36 h, or injected with *beclin1* MO at one-cell stage, showed normal

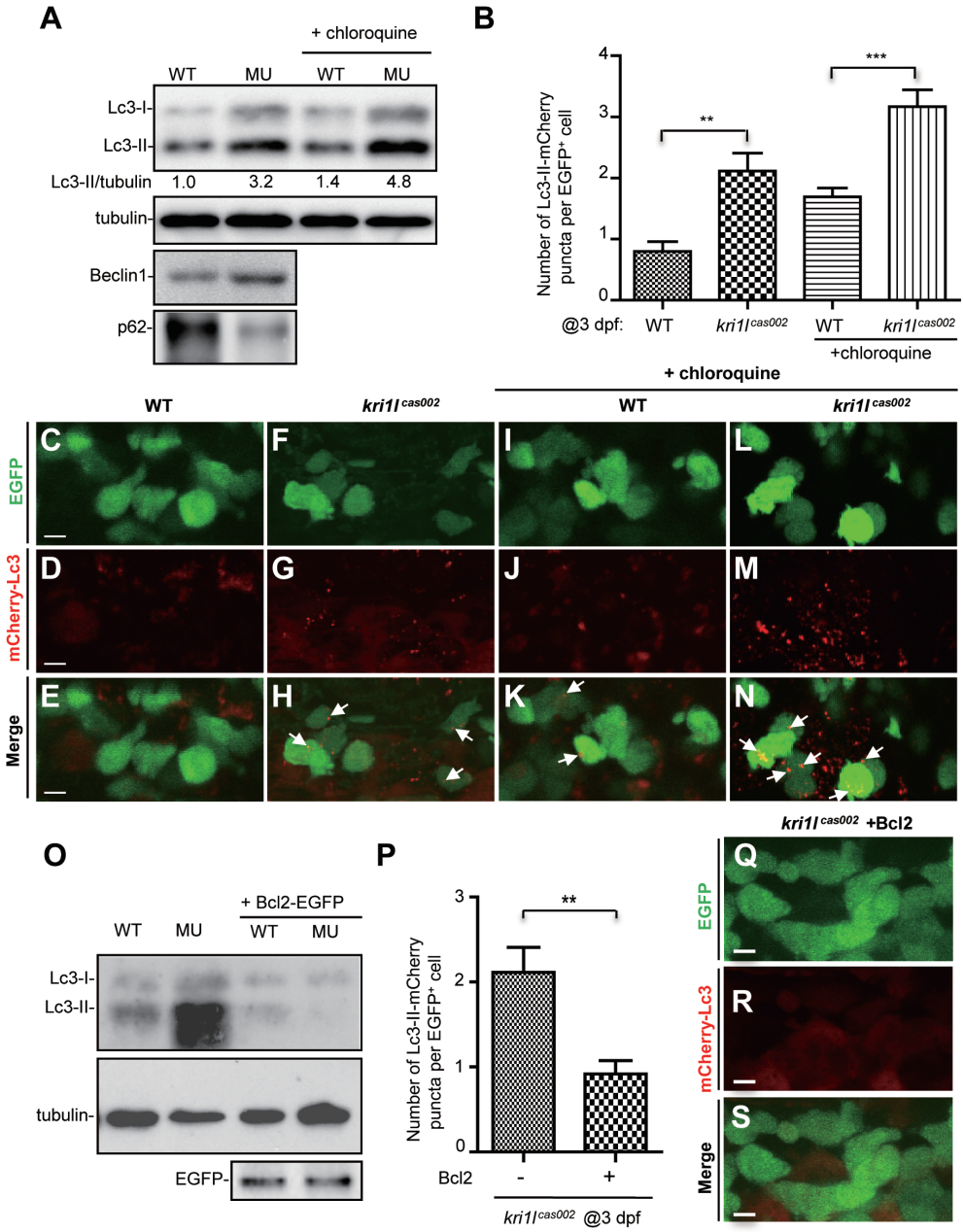

Figure 4 Ectopic expression of Bcl2 inhibits excessive autophagic flux in *kri1l*^{cas002} HSPCs. **(A)** Representative immunoblotting images of Lc3-I, Lc3-II, Beclin1 and p62 in whole embryo lysates of wild-type (WT) and *kri1l*^{cas002} embryos at 3 dpf, treated with or without chloroquine (5 μM) for 6 h before harvest. Tubulin serves as the loading control. **(B)** Statistics of the average number of autophagosome (indicated by mCherry-Lc3 puncta) in *kri1l*^{cas002} mutant embryos and WT siblings with or without chloroquine treatment at 3 dpf. mCherry-Lc3 puncta are counted in over 20 EGFP$^+$ cells (in *cmyb*:*egfp* background) per embryo, total 6-8 embryos under each condition. Without chloroquine treatment, $P = 0.0040$; with chloroquine treatment, $P = 0.0008$. Error bars represent SEM. $^{**}P \le 0.01$; $^{***}P \le 0.001$ (Student's *t*-test). **(C-N)** Representative confocal images of mCherry-Lc3 puncta (autophagosomes) in HSPCs of live zebrafish embryos. Wild type siblings or *kri1l*^{cas002} mutant embryos in the Tg (*cmyb*: *egfp*) transgenic background, were injected with *mcherry-lc3* mRNA at one-cell stage and imaged at 3 dpf with or without pre-treatment with chloroquine (5 μM) for 6 h. Scale bars: 5 μm. **(O)** Immunoblotting analysis of whole embryo lysates from WT and *kri1l*^{cas002} mutant embryos with or without *bcl2* mRNA injection. **(P)** Statistics of the average number of autophagosome for *kri1l*^{cas002} mutant embryos and wild type siblings with Bcl2 overexpression at 3 dpf. mCherry-Lc3 puncta are counted in over 20 EGFP$^+$ (*cmyb*: *egfp*) cells per embryo, total 8-11 individual embryos. $P = 0.0021$. Error bars represent SEM. $^{**}P \le 0.01$; $^{***}P \le 0.001$ (Student's *t*-test). **(Q-S)** Representative confocal images of mCherry-Lc3 puncta (autophagosomes) in HSPCs of live zebrafish embryos with Bcl2 overexpression. Scale bars, 5 μm.

cmyb expression in the CHT (Figure 5A-5E). 3-MA significantly reduced autophagy level in *kri1l*^{cas002} HSPCs, which was visualized by live imaging and quantitation of Lc3-II puncta (Figure 5F-5L; $P = 0.0037$). Furthermore, both Baf A1 (Figure 5M-5U) and 3-MA (data no shown) treatment could restore *kri1l*^{cas002} HSPC proliferation. At 3 dpf, the proportion of pH3^{+}*cmyb*$^{+}$ cells in *kri1l*^{cas002} mutant embryos treated with Baf A1 was almost the same as that in wild type (Figure 5U; $P = 0.2344$). Therefore, inhibition of autophagic flux at different stages is able to rescue HSPC proliferation defects in *kri1l*^{cas002} mutant.

Accumulation of misfolded proteins trigger PERK-dependent autophagy

To understand how Kri1l deficiency-caused ribosome defects trigger excessive autophagy via a p53-independent manner, we hypothesized that impaired ribosome biogenesis might cause dysfunction in protein synthesis to trigger misfolded protein accumulation, which is known to activate autophagy [56, 57].

Protein remodeling factor Hsp110 is known to cooperate with Hsp70 and Hsp40 to dissolve and reactivate aggregated proteins. It is used as a molecular probe to detect puncta foci where misfolded proteins accumulate [58]. We injected an *in vitro* transcribed mRNA coding for Hspa4a (zebrafish homolog of human Hsp110) [59] fused to mCherry into one-cell stage wild-type or *kri1l*^{cas002} embryos stably transgenic for *cmyb*:*egfp*. Abundant Hspa4a-mCherry puncta were observed in *kri1l*^{cas002} EGFP^{+} cells in the CHT region (Figure 6A-6G; $P = 0.0002$), indicating the accumulation of misfolded proteins in Kri1l deficient HSPCs.

Ubiquitination is an important protein post-translational modification, which governs protein quality control. Misfolded or unfolded proteins contain more lysine residues on their surface, and are prone to be recognized and subjected to ubiquitination and degradation [60]. Microinjection of Flag-tagged ubiquitin-expressing construct was performed with or without *kri1l* ATG MO. We found a dramatic accumulation of ubiquitin-modified proteins in *kri1l* ATG morphant (Figure 6H).

Accumulation of misfolded/unfolded proteins is known to trigger activation of PERK, which subsequently phosphorylates eif2a to inhibit protein synthesis [61]. Immunoblotting analysis showed that the phosphorylation level of eif2a protein was indeed upregulated in *kri1l*^{cas002} mutant (Figure 6H). To assess whether PERK signaling plays an important role in the induction of excessive autophagy after the accumulation of unfolded proteins in Kri1l-deficient HSPCs, we treated *kri1l*^{cas002} mutant embryos with PERK-specific inhibitor GSK2656157. GSK2656157 treatment indeed successfully restored the *cmyb* expression in *kri1l*^{cas002} embryos (Figure 6I-6K). Live imaging and immunoblotting analysis further revealed that GSK2656157 treatment inhibited the formation of autophagosomes indicated by LC3-II puncta (Figure 6M-6R and Supplementary information, Figure S18L; $P = 0.0091$). In addition, we performed microinjection of *perk/eif2ak3* MO in *kri1l*^{cas002} mutants. Knockdown of PERK reduced the upregulated level of phosphorylated eif2a (Supplementary information, Figure S19A) and LC3-II (Supplementary information, Figure S19B), meanwhile WISH analysis showed a recovery of *cmyb* expression in *kri1l*^{cas002} embryos (Figure 6I and 6L). These data together support the notion that PERK activation-mediated excessive autophagy in the HSPCs causes hematopoiesis failure in *kri1l*^{cas002}.

Discussion

Through the characterization of a recessive zebrafish mutant *kri1l*^{cas002} with hematopoietic defects we have uncovered a novel connection between ribosome biogenesis and autophagy in HSPCs. Loss of *kri1l* blocks HSPC proliferation in the CHT region and depletes most downstream hematopoietic lineages during definitive hematopoiesis. Due to the dysfunction of SSU complex, in which Kri1l functions as a critical component [41], the level of 18S rRNA is dramatically reduced, although 28S rRNA is spared (Figure 2G-2I). The ribosomal biogenesis defects reduce the rate of protein synthesis (Supplementary information, Figure S9A-S9C) and cause misfolded proteins to aggregate (Figure 6A-6G). Accumulation of misfolded proteins and inefficient protein synthesis trigger PERK activation (Figure 6H), which subsequently upregulates autophagy [56, 57] (Figure 4A, 4C-4N and Supplementary information, Figure S16). Inhibition of autophagy or PERK signaling using drug treatments (Figure 5, 3-MA and Baf A1 targeting autophagy; Figure 6J-6R, GSK2656157 targeting PERK signaling) or MOs (Figure 5D and 5E, targeting *beclin1*; Figure 6I and 6L, targeting *perk*) successfully rescue hematopoiesis defects in *kri1l*^{cas002} mutant embryos.

This finding is distinct from the known regulatory role of apoptosis in bone marrow failure or anemia caused by ribosome disorders [15-18]. Apoptotic signals are normal in HSPCs in the CHT of *kri1l*^{cas002} embryos (Supplementary information, Figure S11). Neither *p53* MO, nor caspase3 inhibitor, nor *p53* null allele, rescued the HSPC defects (Supplementary information, Figure S12, S13A-S13D). Results from our biochemical analyses of Lc3-II level and live imaging of Lc3 puncta in HSPCs, however, attribute hematopoiesis defects in *kri1l*^{cas002} embryos to a hyperactivation of autophagy, which can be inhibited by Bcl2 overexpression that is known to disrupt the formation of VPS34-Beclin1complex during auto-

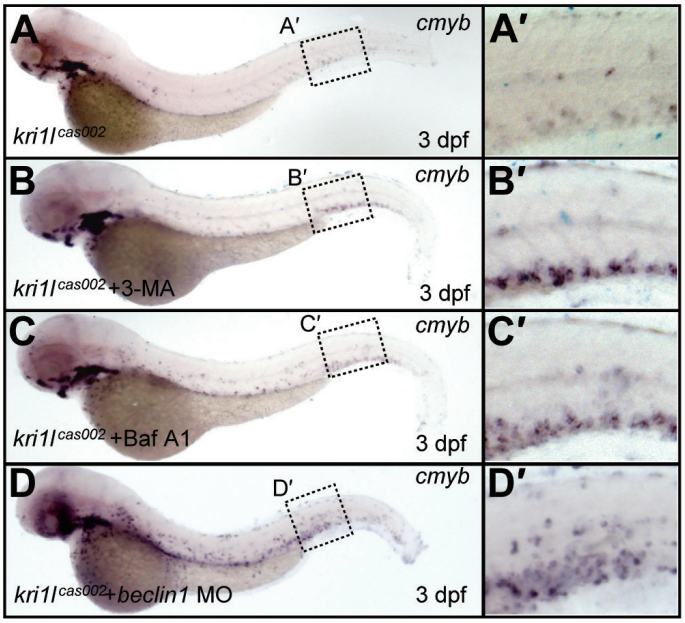
A
A′
cmyb
kri1l cas002
3 dpf
B
B′
kri1l cas002 +3-MA
C
C′
kri1l cas002 +Baf A1
D
D′
kri1l cas002+beclin1 MO

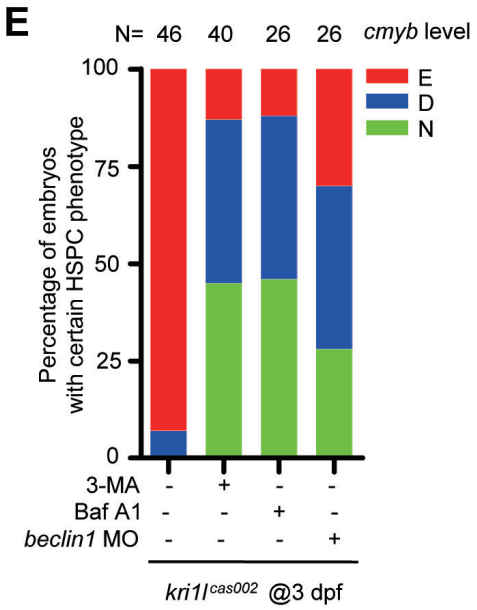
E
N= 46 40 26 26
cmyb level
E
D
N
Percentage of embryos with certain HSPC phenotype
100
75
50
25
0
3-MA - + - -
Baf A1 - - + -
beclin1 MO - - - +
kri1l cas002 @3 dpf

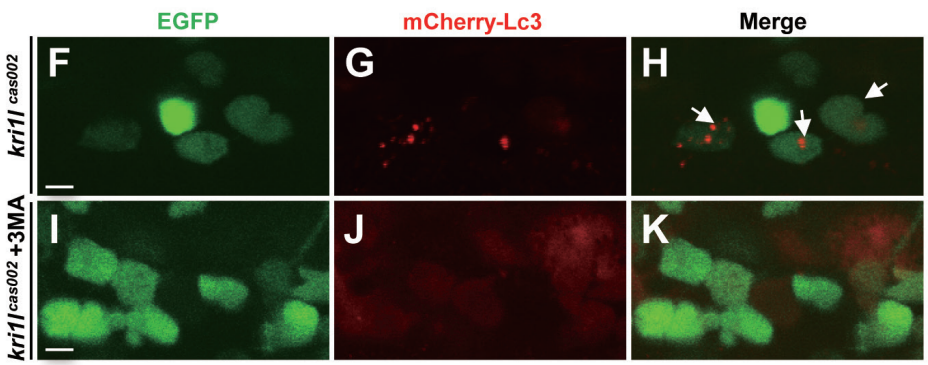
EGFP
mCherry-Lc3
Merge
kri1l cas002
kri1l cas002 +3MA
F
G
H
I
J
K

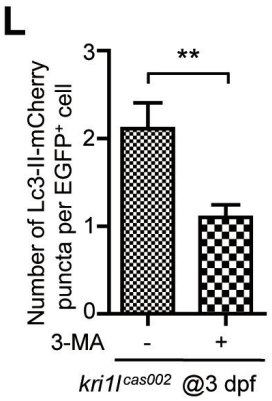
L
Number of Lc3-II-mCherry puncta per EGFP+ cell
3
2
1
0
**
3-MA - +
kri1l cas002 @3 dpf

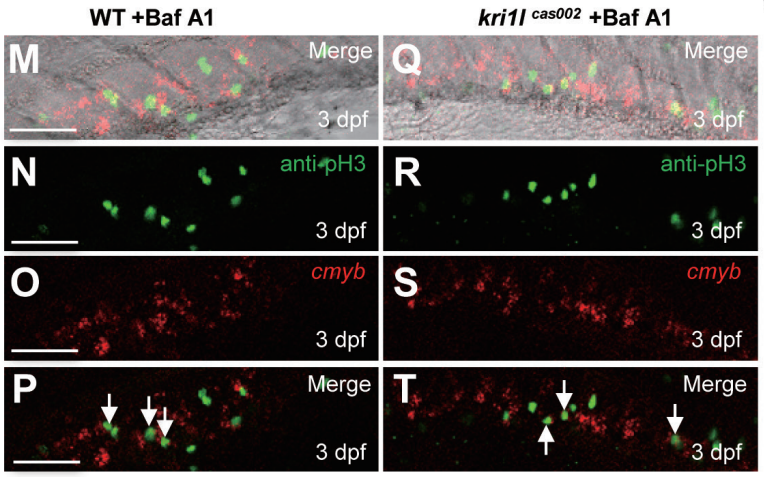
WT +Baf A1
kri1l cas002 +Baf A1
M
Merge
3 dpf
Q
N
anti-pH3
R
O
cmyb
S
P
T

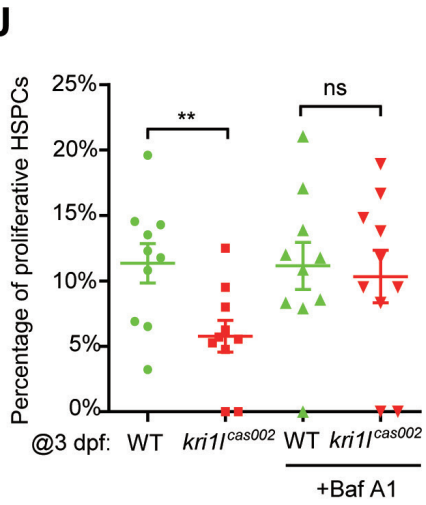
U
Percentage of proliferative HSPCs
25%
20%
15%
10%
5%
0%
**
ns
@3 dpf: WT kri1l cas002 WT kri1l cas002
+Baf A1

phagy initiation [44] (Figure 4B-4N and Supplementary information, Figure S16). We also tested a small molecular compound Z36, which can mimic Beclin1 to competitively interact with Bcl2 [62]. Z36 treatment eliminated *cmyb* expression and increased Lc3-enriched autophagosomes in the CHT region of Bcl2-overexpressed *kri1l*^{cas002} embryos (Supplementary information, Figure S18A-S18K), further supporting the idea that the hematopoietic phenotype in *kri1l*^{cas002} is caused by autophagy that is negatively regulated by Bcl2.

Previous reports have shown that autophagy is essential for HSCs to balance their quiescence, self-renewal and expansion [31]. Activated autophagy driven by FOXO3A-mediated program protects HSCs from starvation-induced apoptosis and maintains HSCs functions [63]. *atg7*$^{-/-}$ HSCs show ROS accumulation and a loss of colony formation capacity in replating [32]. Similar observations are obtained in Atg5 knockdown and in FIP2000-null HSCs [64-66]. In contrast, *kri1l*^{cas002} HSPCs accumulate excessive autophagosomes that are harmful to HSPC proliferation. Our observation and previous reports together suggest that autophagy functions as a double-edged sword [67] in HSPCs, and an appropriate and fine-tuned autophagy level is important for HSPC proliferation and maintenance.

Morrison group has reported that the rate of protein synthesis in HSCs is highly regulated; either increased or decreased protein synthesis impairs HSC function [68]. Naive HSPCs undergo massive expansion upon arrival in CHT. It is conceivable that HSPCs is more sensitive to ribosome disorders due to the proliferative stress associated with the expansion. Indeed, both autophagy level and proliferation status of HSPCs in AGM are normal before their departure for the CHT (Supplementary information, Figure S10A-S10H and Figure S16A-S16F). In addition, cells in other proliferative tissues, such as cranial region and gut, carry more Lc3-mCherry puncta-positive autophagosomes (data not shown). These observations together suggest proliferative state of stem cells may render them particularly sensitive to Kri1l deficiency.

How SSU defects cause the accumulation of misfolded proteins remains elusive. Kri1l deficiency causes defective polysome formation, which includes reduction of functional polysomes or even disassembled polysomes accompanied with excessive 60S subunits. Reduced polysomes or excessive 60S subunits may lead to disorder in protein synthesis, and cause *de novo* synthesis of unproductively folded protein. Especially for larger proteins, the well-coupled translation and folding kinetics are vital for the correct production of functional proteins [69]. Unfolded protein response (UPR) was recently reported to regulate HSCs [70]. *kri1l*^{cas002} HSPCs have a dramatic increase of Hspa4a and ubiquitin-modified proteins, indicating an accumulation of misfolded/unfolded proteins. This leads to the activation of PERK signaling, reflected by an increased level of phospho-eif2a. Importantly, blocking of PERK signaling is sufficient to inhibit excessive autophagy and to rescue definitive hematopoiesis in *kri1l*^{cas002} embryos. However, only the transcription level of *ATF4* (downstream of PERK-eif2a arm of UPR), but not *BIP*, *ATF6*, *chop*, *xbp1* and *xpb1ls* (markers for other signaling arms of UPR), is significantly increased in *kri1l*^{cas002} mutant (Supplementary information, Figure S20D), implying that either only PERK-eif2a signaling cascade is strongly activated in Kri1l deficiency-induced UPR, or excessive autophagy in *kri1l*^{cas002} mutant is triggered by a PERK-dependent, but UPR-independent signaling mechanism.

A model of S6K-mediated inhibition of insulin pathway has been proposed to explain how RPS19 or RPS7 deficiencies induce the upregulation of autophagy level in peripheral blood cells of patients and zebrafish mor-

Figure 5 Autophagy inhibitors prevent hematopoiesis failure in *kri1l*^{cas002} mutant embryos. **(A-D)** Representative images of *cmyb* expression pattern in *kri1l*^{cas002} embryos with or without treatment of autophagy inhibitors, or with microinjection of *beclin1* MO. *kri1l*^{cas002} embryos were treated with 3-MA (10 mM) or Baf A1 (25 nM) from 36 hpf to 72 hpf. After *cmyb* WISH and imaging, all embryos were genotyped; the percentage of the rescue was calculated. 18 out of 40 mutant embryos treated with 3-MA are fully rescued, while 17 out of 40 mutant embryos are rescued partially. 12 out of 26 mutant embryos treated with Baf A1 are fully rescued, while 11 out of 26 mutant embryos are rescued partially. 7 out of 26 mutant embryos injected *beclin1* MO are fully rescued, while 11 out of 26 mutant embryos are rescued partially. **(E)** Percentage of *kri1l*^{cas002} mutant embryos with classified hematopoiesis phenotype with or without treatment of autophagy inhibitors, or with microinjection of *beclin1* MO. **(F-K)** 3-MA inhibits excessive autophagy in HSPCs in *kri1l*^{cas002} mutant embryos. Representative confocal images of mCherry-Lc3 puncta (autophagosomes) in *kri1l*^{cas002} mutant embryos in Tg (*cmyb*:*egfp*) transgenic background are shown. Scale bars, 5 μm. **(L)** Quantitative analysis of **F**-**K**. The numbers of autophagosomes are decreased in *kri1l*^{cas002} embryos with 3-MA treatment, $p = 0.0037$. **(M-T)** Baf A1 treatment restores HSPCs proliferation in *kri1l*^{cas002} mutant embryos. Double staining of *cmyb* RNA (red) and phospho-histone 3 (pH3) protein (green) in the CHT region of embryos at 3 dpf. **M** and **Q** show bright-field images overlaid with fluorescent staining. Scale bars, 50 μm. **(U)** Percentage of proliferative HSPCs in the CHT of *kri1l*^{cas002} mutant embryos and wild type siblings with or without Baf A1 treatment at 3 dpf $N = 10$. Without Baf A1 treatment, $p = 0.0014$; with Baf A1 treatment, $P = 0.2344$. Error bars represent SEM. $^{**}P \leq 0.01$; $^{***}P \leq 0.001$ (Student's *t*-test).

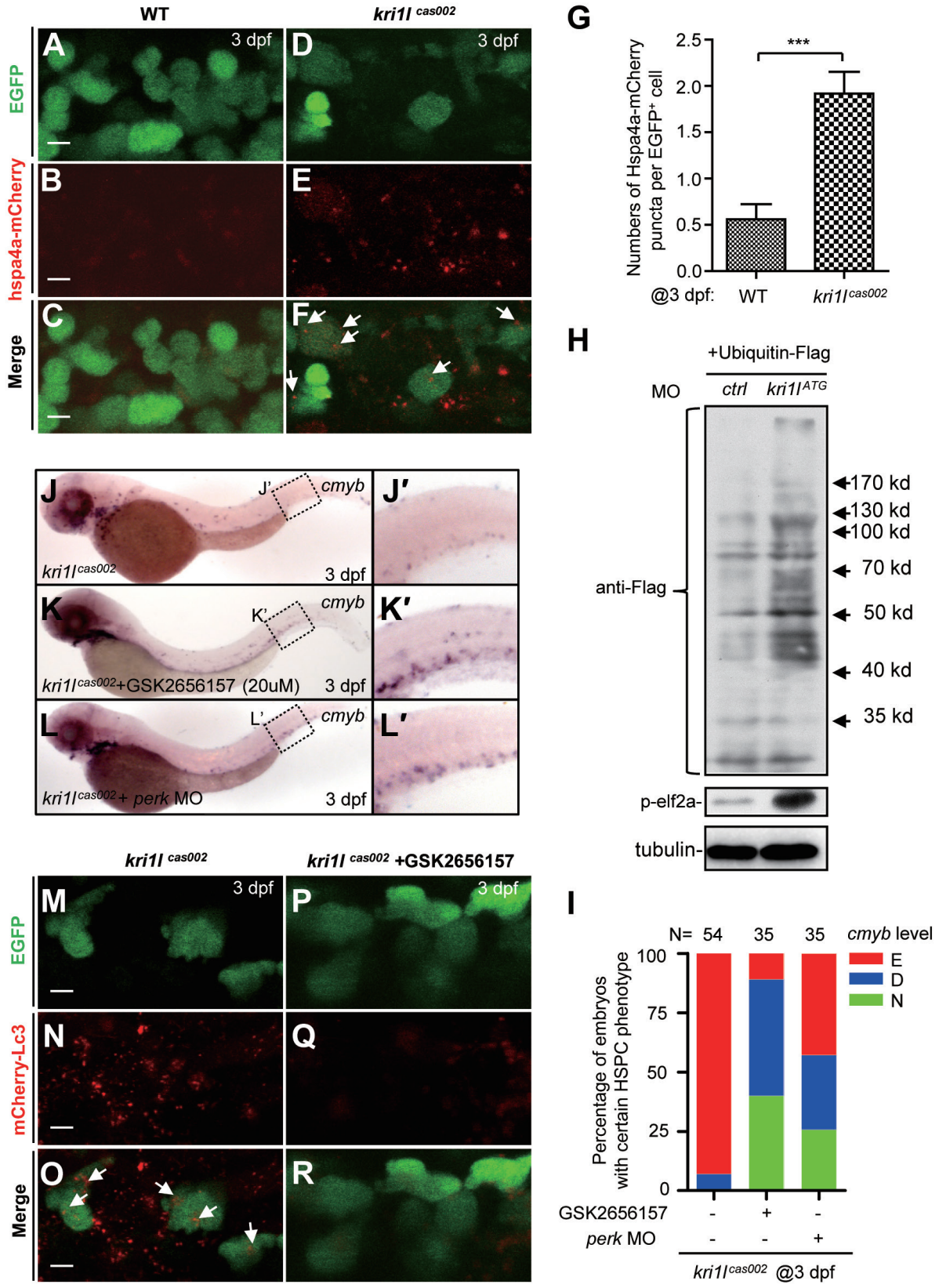
WT
kri1l cas002
EGFP
hspa4a-mCherry
Merge
A
3 dpf
D
3 dpf
B
E
C
F
G
Numbers of Hspa4a-mCherry puncta per EGFP+ cell
2.5
2.0
1.5
1.0
0.5
0.0
***
@3 dpf:
WT
kri1l cas002
H
+Ubiquitin-Flag
MO
ctrl
kri1l ATG
anti-Flag
170 kd
130 kd
100 kd
70 kd
50 kd
40 kd
35 kd
p-elf2a-
tubulin-
J
J'
cmyb
kri1l cas002
3 dpf
K
K'
kri1l cas002+GSK2656157 (20uM)
3 dpf
L
L'
kri1l cas002+ perk MO
3 dpf
kri1l cas002
kri1l cas002 +GSK2656157
M
3 dpf
P
3 dpf
mCherry-Lc3
N
Q
Merge
O
R
I
N= 54 35 35
cmyb level
E
D
N
Percentage of embryos with certain HSPC phenotype
100
75
50
25
0
GSK2656157
perk MO
kri1l cas002 @3 dpf

phants [38]. We also show an upregulation of S6K and its downstream effector-RPS6 in *kri1l*^{cas002} mutant embryos (Supplementary information, Figure S22A). However, phospho-RPS6 signaling is dominant in peripheral blood cells, but not in EGFP$^+$ HSPCs in either wild-type or *kri1l*^{cas002} mutant (Supplementary information, Figure S22C-S22K), suggesting S6K was not the major regulator to induce excessive autophagy in *kri1l*^{cas002} HSPCs. Taken together, we propose that the deficiency of Kri1l causes an impaired ribosome biogenesis, resulting in the accumulation of misfolded proteins. Aggregation of misfolded proteins activates PERK signaling, which in turn triggers a significant increase of autophagy. Excessive autophagy finally leads to an inhibition of definitive hematopoiesis. The S6K-RPS6 axis might be involved in the regulation of Kri1l-deficient peripheral blood cells rather than HSPCs (Supplementary information, Figure S22B). In addition, we found that rapamycin treatment could not rescue hematopoietic failure phenotype in *kri1l* mutant (Supplementary information, Figure S20A-S20C).

Although *lmo2* promoter-induced expression of wild-type Kri1l rescued defective hematopoiesis in *kri1l*^{cas002} embryos (Supplementary information, Figure S21), suggesting a cell autonomous role of Kri1l in HSPCs, it is also worth to note the presence of other cell types in the CHT. These include niche cells forming the hematopoietic microenvironment and differentiated hematopoietic lineage cells. They may also undergo an upregulation of autophagic flux in *kri1l*^{cas002} mutant. Since appropriate cell-cell interactions in hematopoietic niche are vital for HSPC self-renewal, non-cell autonomous effects may also contribute to the defective hematopoiesis in *kri1l*^{cas002} mutant.

In conclusion, an intact ribosome biogenesis, optimal protein synthesis and an appropriate level of autophagy are critical for HSPC maintenance and proliferation. During the first wave of HSPC expansion in the CHT region, a higher level of protein synthesis is needed, which makes HSPCs more sensitive to dysfunctional ribosome biogenesis [68, 71]. In *kri1l*^{cas002} HSPCs, impaired ribosome biogenesis causes ribosomal stress and an upregulation of autophagy, which subsequently results in impaired proliferation of HSPCs. Decreased HSPCs can be restored by the treatment of autophagy inhibitors, PERK inhibitor and PERK/Beclin1 knockdown (Figure 7). This study suggests that autophagy level may be useful for the clinical diagnosis of anemia or bone marrow failure caused by ribosomopathies. Our finding also suggests patients with certain types of ribosomopathy may benefit from treatments with autophagy inhibitors, such as lys05 or spautin-1 [71]. In addition, the mechanism revealed in this study may also play an important role in the progression of other human diseases caused by ribosome abnormalities.

Materials and Methods

Zebrafish husbandry and MO/mRNA microinjection

Zebrafish stock maintenance, ENU mutagenesis and positional cloning were performed as previously described [39, 72, 73]. Zebrafish facility and study were approved by Institutional Animal Use Review Board of Institute of Health Sciences, Shanghai Institutes of Biological Sciences, Chinese Academy of Sciences. Morpholino oligonucleotides (MOs) were ordered from Gene Tools, LLC. Capped mRNAs were transcribed from linearized pCS2$^+$ plasmids (mMessage Machine; Ambion), purified and diluted to 150 ng/μl for microinjection into zebrafish embryos at 1-cell stage.

ENU mutagenesis and positional cloning

ENU mutagenesis and positional cloning were performed as previously described [39, 72]. The *cas002* (Tu background) allele

Figure 6 Accumulation of unfolded proteins and PERK activation leads to excessive autophagy and hematopoiesis failure. **(A-G)** Representative confocal images **(A-F)** and Quantitation **(G)** of Hspa4a-mCherry puncta (aggregation of misfolded protein) in HSPCs of live zebrafish embryos. Wild-type siblings or *kri1l*^{cas002} mutant embryos in the Tg (*cmyb*:*egfp*) transgenic background were injected with *hspa4a-mcherry* mRNA at one-cell stage and imaged at 3 dpf. The numbers of misfolded protein puncta are increased in *kri1l*^{cas002} embryos compared to that in wild-type siblings, $P = 0.0002$. Hspa4a-mCherry puncta were counted in over 30 EGFP$^+$ cells (in the Tg (*cmyb*: *egfp*) background) per embryo, total 10-12 embryos. Error bars represent SEM. $^{**}P \le 0.01$; $^{***}P \le 0.001$ (Student's *t*-test). Scale bars, 5 μm. **(H)** Representative immunoblotting analysis of the level of protein ubiquitination and phospho-eif2a in whole embryo lysates of WT and *kri1l*^{cas002} embryos at 3 dpf injected with Flag-tagged ubiquitin plasmid at one-cell stage. Tubulin serves as the loading control. **(I)** Treatment with PERK inhibitor GSK2656157 or injection of *perk* MO rescues *cmyb* expression in HSPCs. *Kri1l*^{cas002} mutant embryos were treated with GSK2656157 (20 μM) from 36 hpf to 72 hpf, or injected with *perk* MO at one-cell stage. After WISH and imaging, all embryos were genotyped. 14 out of 35 mutant embryos treated with GSK2656157 are fully rescued, while 17 out of 35 mutant embryos are rescued partially. 9 out of 35 mutant embryos injected with *perk* MO are fully rescued, while 11 out of 35 mutant embryos are rescued partially. **(J-L)** Proportion of *kri1l*^{cas002} mutant embryos with classified hematopoiesis phenotype with or without GSK2656157 treatment, or with microinjection of *perk* MO. **(M-R)** GSK2656157 inhibits excessive autophagy in *kri1l*^{cas002} HSPCs. Representative confocal images of mCherry-Lc3 puncta (autophagosomes) in *kri1l*^{cas002} mutant embryos in Tg (*cmyb*:*egfp*) transgenic background are shown. Scale bars, 5 μm.

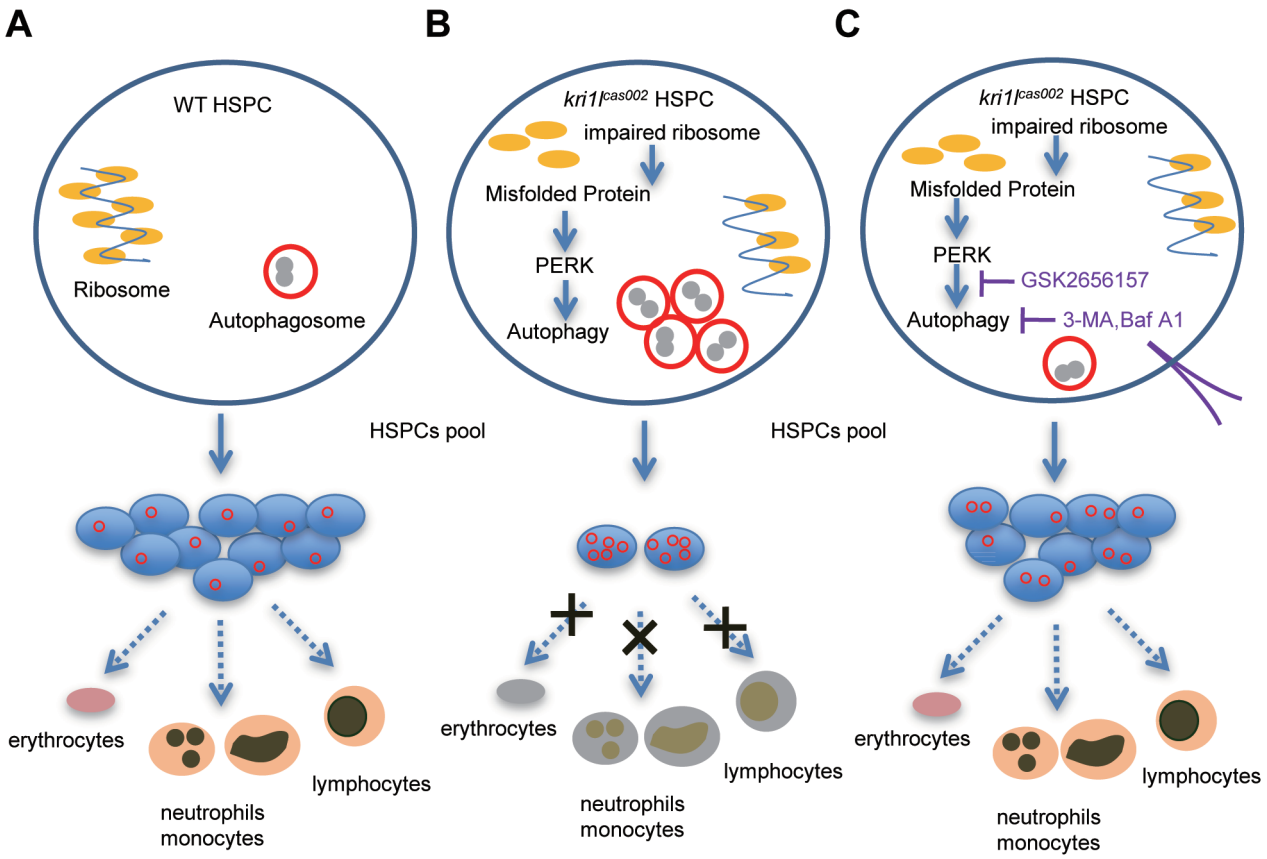

Figure 7 Working model for Kri1l dysfunction-induced hematopoietic defects and its treatment. **(A)** In normal HSPCs, ribosome biogenesis is tightly regulated; autophagy occurs at an appropriate level. HSPCs expand massively in the CHT region and differentiate into multiple hematopoietic lineages, including erythrocytes, myeloid cells (neutrophils and monocytes) and lymphocytes. **(B)** In *kri1l*^{cas002} HSPCs, abnormal ribosome biogenesis leads to the accumulation of misfolded proteins, which triggers PERK activation and excessive autophagy. The excessive autophagy leads to inhibition of HPSC proliferation, depletion of HSPC pool, and a profound hematopoiesis failure. **(C)** Blocking of PERK signaling with specific inhibitor (GSK2656157), Bcl2 overexpression or treatment with autophagy inhibitors (3-MA, Baf A1) reduces autophagy level and restores HSPC proliferation defects and hematopoietic lineage differentiation in *kri1l*^{cas002} mutant embryo.

was mapped by out-crossing Tu background heterozygous fish into polymorphic WIK background wild-type strain. We scanned the genome for linked SSLP markers by BSA. SSLP markers [74, 75] used for BSA were selected from the Massachusetts General Hospital Zebrafish Server website (http://zebrafish.mgh.harvard.edu). Fine mapping using mainly SSLP markers was carried out to narrow down the genetic interval. The cDNAs of candidate genes in the interval were cloned and sequenced from pooled mutants, and candidate mutation was confirmed by sequencing genomic DNA of individual mutant embryo. All primers used for this study are provided in Supplementary Table 1.

WISH, TUNEL assay and immunostaining

Antisense RNA probes were transcribed using linearized constructs with T3 or T7 polymerase (Ambion) in the presence of digoxigenin (DIG, Roche)-labeled UTP using the DIG-RNA Labeling Kit (Roche). WISH was performed as described previously using NBT/BCIP (Sigma) as substrates [76, 77]. TUNEL was performed with *In Situ* Cell Death Detection Kit and TMR Red Kit (Roche) following manufacturer's instruction. To detect both *cmyb* RNA and mitosis marker pH3 simultaneously, embryos were first hybridized with the DIG-labeled antisense *cmyb* RNA probe, incubated at 4 °C overnight with a peroxidase-conjugated anti-DIG antibody (1:500; Roche), and stained with Alexa Fluor cy3-conjugated tyramide as substrate (PerkinElmer). The embryos were then incubated with primary anti-pH3 (ser10) antibody (1:500; Santa Cruz), and finally incubated with Alexa Fluor 488-labeled goat anti-rabbit IgG antibody (1:500; Invitrogen).

Plasmid construction

The zebrafish cDNA of *kri1l* gene was amplified from reverse transcription products and cloned into pCS2^{+} vector. For construction of the *kri1l* (1-60)-*gfp* reporter plasmid, the zebrafish cDNA (1-60 aa) of *kri1l* gene was amplified and cloned into pCS2^{+}-*egfp* vector. For construction of Tg (*lmo2:kri1l*) transient transgenesis plasmid, the zebrafish *lmo2* promoter was obtained by PCR amplification from *lmo2-Cre-PBSK-I-SceI* plasmid, and then cloned into the Tol2 transposon backbone together with full-length *kri1l* gene

[78]. For construction of the *mcherry-lc3* plasmid, the PCR was performed to generate *mcherry* cDNA without the termination codon, and then replace the EGFP coding region of pEGFP-C1, and the resulting plasmid was named mCherry-C1. The fragment of *lc3* was inserted into the corresponding sites in the mCherry-C1 plasmid. The zebrafish cDNA of *hspa4a* gene without the termination codon was amplified and cloned into $pCS2^+$ vector. Then *mcherry* cDNA was generated by PCR and inserted into $pCS2^+$-*hspa4a*.

Live imaging of autophagy and unfolded protein in HSPCs

mCherry-Lc3 mRNA or *hspa4a-mCherry* mRNA was transcribed via the mMessage mMachine SP6 kit (Ambion), and then injected into Tg (*cmyb*:*egfp*) transgenic zebrafish embryos at one-cell stage. The live embryos were anesthetized with tricaine and mounted in 3% low melting point agarose for imaging with Olympus FV1000 scanning confocal microscope (under a 60×/1.00 NA water-immersion objective) [79].

Immunoblotting analysis

Embryos were deyolked [80], and then homogenized in lysis buffer (20 mM Tris-HCl (pH 7.4), 150 mM NaCl, 5 mM EDTA, 10% glycerol, 0.1% Triton X-100, protease inhibitor cocktail and phosphatase inhibitor (Roche)). Protein lysates were separated on SDS-PAGE, transferred to nitrocellulose membrane (Amersham Biosciences), and incubated with anti-LC3 (Cell Signaling Technology, 1:1 000), phos-S6K (Cell Signaling Technology, 1:1 000), phos-RPS6 (Cell Signaling Technology, 1:1 000), phos-elf2a (Cell Signaling Technology, 1:1 000), p62 (MBL,1:1 000), Beclin1 (abcam, 1:5 000), p53 (a gift from Jinrong Peng, Zhejiang University) or anti-α-tubulin (Sigma, 1:2 000) antibodies, and then HRP-conjugated secondary Antibodies.

Small molecular compound treatment

Final concentrations of chemicals used in this study were 5 μM chloroquine (Fluka Sigma-Aldrich), 10 mM 3-MA (Sigma), 25 nM Baf A1 (Santa Cruz), 10 μM Z36 (Sigma) and 20 μM GSK2656157 (Selleck). Embryos were incubated with small molecular chemicals in embryo medium at 28.5 °C until collection.

Transmission electron microscopy

For electron microscopy analysis, 3 dpf zebrafish embryos were fixed in a mixture of 2% paraformaldehyde and 0.2% glutaraldehyde in 0.1 M phosphate buffer. The embryos were washed in PBS-glycine to quench free aldehydes, then embedded in gelatin and infiltrated in 2.3 M sucrose, and subjected to rapid freezing in liquid N_2. 50 nM thick cryosections were cut at −120 °C using an Ultracut-S ultra microtome (Leica Microsystems). Sections were directly viewed in a FEI Tecnai G2 Spirit Twin electron microscope (FEI).

Quantitative PCR analysis

Total RNAs were extracted from 20 zebrafish embryos using Trizol reagent (Invitrogen). RNA was reverse-transcribed using random hexamers and SuperScript III Reverse Transcriptase (Invitrogen). 2× PCR Mix (TaKaRa, Premix Ex Taq) containing SYBR Green I was used for the real-time quantitative PCR analysis with the Applied Biosystems 7900HT Fast Real-Time PCR System. The relative expression values were normalized against the internal control actin (QPCR primer sequences were listed in Supplementary information, Table S1).

Quantitation of rRNA and polysome level

As previously described [21], total RNA was extracted from WT or *kri1l*^{cas002} mutant zebrafish and then analyzed on an Agilent 2100 E-Bioanalyser according to the manufacturer's instructions. 140 WT or *kri1l*^{cas002} larvae at 72 hpf were deyolked, washed and resuspended in cold lysis buffer (50 mM Tris-HCl (pH 7.4), 150 mM KCl, 10 mM MgCL2, 1% Triton X-100, 2 mM DTT, 0.5% sodium deoxycholate and 0.1 mg/ml cycloheximide) containing 100 U/ml RNase inhibitor (Promega), Complete Protease Inhibitor Cocktail (Roche), sodium vanadate, sodium fluoride and PMSF. Next, samples were homogenized by small pestles. Lysates were incubated on ice for 15 min and centrifuged (12 000 rpm, 10 min at 4 °C) to pellet the nuclei and cellular debris. The supernatant of each sample was loaded onto a continuous 15% - 45% (w/v) sucrose gradient in high salt resolving buffer (20 mM HEPES (pH7.4), 150 mM KCl, and 10 mM MgCl2) generated by a Biocomp gradient master. The mixture was next centrifuged in a Beckman SW41ti rotor (Beckman Coulter) at 36 000 rpm for 3.5 h at 4 °C, and the absorbance at 254 nm was determined with an EM-1 UV Monitor (Bio-Rad).

Acknowledgment

We thank Xiaolan Peng, Ting-Xi Liu, Jinrong Peng, Zhixue Liu, Wei-Li Zhao, Jiang Zhu, Jing-Yi Shi, Qing Chen, Li-Ting Chen, Fan Yang and Zhong Zheng for technical support and suggestions. This work was supported by grants from National Natural Science Foundation of China (31371461 to WJP, 81123005 to State Key Laboratory for Medical Genomics, 31301209 to CBJ, 31301196 to MD), Inner Mongolia Natural Science Foundation (2015BS0801 to XEJ), Science and Technology Commission of Shanghai Municipality (13JC1406400) and National Thousand Talents Program for Distinguished Young Scholars to WJP.

References

1 Galloway JL, Zon LI. Ontogeny of hematopoiesis: examining the emergence of hematopoietic cells in the vertebrate embryo. *Curr Top Dev Biol* 2003; **53**:139-158.
2 Orkin SH, Zon LI. Hematopoiesis: an evolving paradigm for stem cell biology. *Cell* 2008; **132**:631-644.
3 Morrison SJ, Uchida N, Weissman IL. The biology of hematopoietic stem cells. *Annu Rev Cell Dev Biol* 1995; **11**:35-71.
4 Bertrand JY, Traver D. Hematopoietic cell development in the zebrafish embryo. *Curr Opin Hematol* 2009; **16**:243-248.
5 Paw BH, Zon LI. Zebrafish: a genetic approach in studying hematopoiesis. *Curr Opin Hematol* 2000; **7**:79-84.
6 Song HD, Sun XJ, Deng M, *et al.* Hematopoietic gene expression profile in zebrafish kidney marrow. *Proc Natl Acad Sci USA* 2004; **101**:16240-16245.
7 Bertrand JY, Kim AD, Teng S, Traver D. CD41+ cmyb+ precursors colonize the zebrafish pronephros by a novel migration route to initiate adult hematopoiesis. *Development* 2008; **135**:1853-1862.
8 Jin H, Xu J, Wen Z. Migratory path of definitive hematopoietic stem/progenitor cells during zebrafish development. *Blood* 2007; **109**:5208-5214.

9 Kissa K, Murayama E, Zapata A, *et al*. Live imaging of emerging hematopoietic stem cells and early thymus colonization. *Blood* 2008; **111**:1147-1156.
10 Murayama E, Kissa K, Zapata A, *et al.* Tracing hematopoietic precursor migration to successive hematopoietic organs during zebrafish development. *Immunity* 2006; **25**:963-975.
11 Sondalle SB, Baserga SJ. Human diseases of the SSU processome. *Biochim Biophys Acta* 2014; **1842**:758-764.
12 Liu JM, Ellis SR. Ribosomes and marrow failure: coincidental association or molecular paradigm? *Blood* 2006; **107**:4583-4588.
13 Narla A, Ebert BL. Ribosomopathies: human disorders of ribosome dysfunction. *Blood* 2010; **115**:3196-3205.
14 Aguissa-Toure AH, Da Costa L, Leblanc T, Tchernia G, Fribourg S, Gleizes PE. Diamond-Blackfan anemia reveals the dark side of ribosome biogenesis. *Med Sci (Paris)* 2009; **25**:69-76.
15 Taylor AM, Humphries JM, White RM, Murphey RD, Burns CE, Zon LI. Hematopoietic defects in rps29 mutant zebrafish depend upon p53 activation. *Exp Hematol* 2012; **40**:228-237.
16 Barlow JL, Drynan LF, Hewett DR, *et al.* A p53-dependent mechanism underlies macrocytic anemia in a mouse model of human 5q- syndrome. *Nat Med* 2010; **16**:59-66.
17 McGowan KA, Li JZ, Park CY, *et al.* Ribosomal mutations cause p53-mediated dark skin and pleiotropic effects. *Nat Genet* 2008; **40**:963-970.
18 Danilova N, Sakamoto KM, Lin S. Ribosomal protein S19 deficiency in zebrafish leads to developmental abnormalities and defective erythropoiesis through activation of p53 protein family. *Blood* 2008; **112**:5228-5237.
19 Chakraborty A, Uechi T, Higa S, Torihara H, Kenmochi N. Loss of ribosomal protein L11 affects zebrafish embryonic development through a p53-dependent apoptotic response. *PLoS One* 2009; **4**:e4152.
20 Provost E, Wehner KA, Zhong X, *et al.* Ribosomal biogenesis genes play an essential and p53-independent role in zebrafish pancreas development. *Development* 2012; **139**:3232-3241.
21 Boglev Y, Badrock AP, Trotter AJ, *et al.* Autophagy induction is a Tor- and Tp53-independent cell survival response in a zebrafish model of disrupted ribosome biogenesis. *PLoS Genet* 2013; **9**:e1003279.
22 Torihara H, Uechi T, Chakraborty A, Shinya M, Sakai N, Kenmochi N. Erythropoiesis failure due to RPS19 deficiency is independent of an activated Tp53 response in a zebrafish model of Diamond-Blackfan anaemia. *Br J Haematol* 2011; **152**:648-654.
23 Dutt S, Narla A, Lin K, *et al.* Haploinsufficiency for ribosomal protein genes causes selective activation of p53 in human erythroid progenitor cells. *Blood* 2011; **117**:2567-2576.
24 Zhang Y, Duc AC, Rao S, *et al.* Control of hematopoietic stem cell emergence by antagonistic functions of ribosomal protein paralogs. *Dev Cell* 2013; **24**:411-425.
25 Hara T, Nakamura K, Matsui M, *et al.* Suppression of basal autophagy in neural cells causes neurodegenerative disease in mice. *Nature* 2006; **441**:885-889.
26 Komatsu M, Waguri S, Chiba T, *et al.* Loss of autophagy in the central nervous system causes neurodegeneration in mice. *Nature* 2006; **441**:880-884.
27 Espina V, Liotta LA. What is the malignant nature of human ductal carcinoma in situ? *Nat Rev Cancer* 2011; **11**:68-75.
28 Degenhardt K, Mathew R, Beaudoin B, *et al.* Autophagy promotes tumor cell survival and restricts necrosis, inflammation, and tumorigenesis. *Cancer Cell* 2006; **10**:51-64.
29 He C, Klionsky DJ. Regulation mechanisms and signaling pathways of autophagy. *Annu Rev Genet* 2009; **43**:67-93.
30 Funderburk SF, Wang QJ, Yue Z. The Beclin 1-VPS34 complex--at the crossroads of autophagy and beyond. *Trends Cell Biol* 2010; **20**:355-362.
31 Guan JL, Simon AK, Prescott M, *et al.* Autophagy in stem cells. *Autophagy* 2013; **9**:830-849.
32 Mortensen M, Soilleux EJ, Djordjevic G, *et al.* The autophagy protein Atg7 is essential for hematopoietic stem cell maintenance. *J Exp Med* 2011; **208**:455-467.
33 Miller BC, Zhao Z, Stephenson LM, *et al*. The autophagy gene ATG5 plays an essential role in B lymphocyte development. *Autophagy* 2008; **4**:309-314.
34 Pua HH, Dzhagalov I, Chuck M, Mizushima N, He YW. A critical role for the autophagy gene Atg5 in T cell survival and proliferation. *J Exp Med* 2007; **204**:25-31.
35 Kundu M, Lindsten T, Yang CY, *et al.* Ulk1 plays a critical role in the autophagic clearance of mitochondria and ribosomes during reticulocyte maturation. *Blood* 2008; **112**:1493-1502.
36 Mortensen M, Ferguson DJ, Edelmann M, *et al.* Loss of autophagy in erythroid cells leads to defective removal of mitochondria and severe anemia *in vivo*. *Proc Natl Acad Sci USA* 2010; **107**:832-837.
37 Sandoval H, Thiagarajan P, Dasgupta SK, *et al.* Essential role for Nix in autophagic maturation of erythroid cells. *Nature* 2008; **454**:232-235.
38 Heijnen HF, van Wijk R, Pereboom TC, *et al.* Ribosomal protein mutations induce autophagy through S6 kinase inhibition of the insulin pathway. *PLoS Genet* 2014; **10**:e1004371.
39 Bahary N, Davidson A, Ransom D, *et al.* The Zon laboratory guide to positional cloning in zebrafish. *Methods Cell Biol* 2004; **77**:305-329.
40 Whitehead GG, Makino S, Lien CL, Keating MT. fgf20 is essential for initiating zebrafish fin regeneration. *Science* 2005; **310**:1957-1960.
41 Sasaki T, Toh EA, Kikuchi Y. Yeast Krr1p physically and functionally interacts with a novel essential Kri1p, and both proteins are required for 40S ribosome biogenesis in the nucleolus. *Mol Cell Biol* 2000; **20**:7971-7979.
42 Yuan H, Zhou J, Deng M, *et al.* Small ubiquitin-related modifier paralogs are indispensable but functionally redundant during early development of zebrafish. *Cell Res* 2010; **20**:185-196.
43 Chen J, Ng SM, Chang C, *et al.* p53 isoform delta113p53 is a p53 target gene that antagonizes p53 apoptotic activity via BclxL activation in zebrafish. *Genes Dev* 2009; **23**:278-290.
44 Pattingre S, Tassa A, Qu X, *et al.* Bcl-2 antiapoptotic proteins inhibit Beclin 1-dependent autophagy. *Cell* 2005; **122**:927-939.
45 Maiuri MC, Le Toumelin G, Criollo A, *et al.* Functional and physical interaction between Bcl-X(L) and a BH3-like domain in Beclin-1. *EMBO J* 2007; **26**:2527-2539.
46 Klionsky DJ, Abdalla FC, Abeliovich H, *et al.* Guidelines for the use and interpretation of assays for monitoring autophagy.

Autophagy 2012; **8**:445-544.
47 Klionsky DJ, Abeliovich H, Agostinis P, *et al.* Guidelines for the use and interpretation of assays for monitoring autophagy in higher eukaryotes. *Autophagy* 2008; **4**:151-175.
48 Berghmans S, Murphey RD, Wienholds E, *et al.* tp53 mutant zebrafish develop malignant peripheral nerve sheath tumors. *Proc Natl Acad Sci USA* 2005; **102**:407-412.
49 Galavotti S, Bartesaghi S, Faccenda D, *et al.* The autophagy-associated factors DRAM1 and p62 regulate cell migration and invasion in glioblastoma stem cells. *Oncogene* 2013; **32**:699-712.
50 He C, Klionsky DJ. Analyzing autophagy in zebrafish. *Autophagy* 2010; **6**:642-644.
51 He C, Bartholomew CR, Zhou W, Klionsky DJ. Assaying autophagic activity in transgenic GFP-Lc3 and GFP-Gabarap zebrafish embryos. *Autophagy* 2009; **5**:520-526.
52 Kimmelman AC. The dynamic nature of autophagy in cancer. *Genes Dev* 2011; **25**:1999-2010.
53 Schonewolf CA, Mehta M, Schiff D, *et al.* Autophagy inhibition by chloroquine sensitizes HT-29 colorectal cancer cells to concurrent chemoradiation. *World J Gastrointest Oncol* 2014; **6**:74-82.
54 Wu YT, Tan HL, Shui G, *et al.* Dual role of 3-methyladenine in modulation of autophagy via different temporal patterns of inhibition on class I and III phosphoinositide 3-kinase. *J Biol Chem* 2010; **285**:10850-10861.
55 Yamamoto A, Tagawa Y, Yoshimori T, Moriyama Y, Masaki R, Tashiro Y. Bafilomycin A1 prevents maturation of autophagic vacuoles by inhibiting fusion between autophagosomes and lysosomes in rat hepatoma cell line, H-4-II-E cells. *Cell Struct Funct* 1998; **23**:33-42.
56 Hoyer-Hansen M, Jaattela M. Connecting endoplasmic reticulum stress to autophagy by unfolded protein response and calcium. *Cell Death Differ* 2007; **14**:1576-1582.
57 Kouroku Y, Fujita E, Tanida I, *et al.* ER stress (PERK/eIF2alpha phosphorylation) mediates the polyglutamine-induced LC3 conversion, an essential step for autophagy formation. *Cell Death Differ* 2007; **14**:230-239.
58 Buchberger A, Bukau B, Sommer T. Protein quality control in the cytosol and the endoplasmic reticulum: brothers in arms. *Mol Cell* 2010; **40**:238-252.
59 Crawford KC, Vega Flores M, Oehlers SH, Hall CJ, Crosier KE, Crosier PS. Zebrafish heat shock protein a4 genes in the intestinal epithelium are up-regulated during inflammation. *Genesis* 2011; **49**:905-911.
60 Amm I, Sommer T, Wolf DH. Protein quality control and elimination of protein waste: the role of the ubiquitin-proteasome system. *Biochim Biophys Acta* 2014; **1843**:182-196.
61 Wek RC, Cavener DR. Translational control and the unfolded protein response. *Antioxid Redox Signal* 2007; **9**:2357-2371.
62 Lin J, Zheng Z, Li Y, *et al.* A novel Bcl-XL inhibitor Z36 that induces autophagic cell death in Hela cells. *Autophagy* 2009; **5**:314-320.
63 Warr MR, Binnewies M, Flach J, *et al.* FOXO3A directs a protective autophagy program in haematopoietic stem cells. *Nature* 2013; **494**:323-327.
64 Salemi S, Yousefi S, Constantinescu MA, Fey MF, Simon HU. Autophagy is required for self-renewal and differentiation of adult human stem cells. *Cell Res* 2012; **22**:432-435.
65 Liu F, Guan JL. FIP200, an essential component of mammalian autophagy is indispensible for fetal hematopoiesis. *Autophagy* 2011; **7**:229-230.
66 Liu F, Lee JY, Wei H, *et al.* FIP200 is required for the cell-autonomous maintenance of fetal hematopoietic stem cells. *Blood* 2010; **116**:4806-4814.
67 Shintani T, Klionsky DJ. Autophagy in health and disease: a double-edged sword. *Science* 2004; **306**:990-995.
68 Signer RA, Magee JA, Salic A, Morrison SJ. Haematopoietic stem cells require a highly regulated protein synthesis rate. *Nature* 2014; **509**:49-54.
69 Kim YE, Hipp MS, Bracher A, Hayer-Hartl M, Hartl FU. Molecular chaperone functions in protein folding and proteostasis. *Annu Rev Biochem* 2013; **82**:323-355.
70 van Galen P, Kreso A, Mbong N, *et al.* The unfolded protein response governs integrity of the haematopoietic stem-cell pool during stress. *Nature* 2014; **510**:268-272.
71 McAfee Q, Zhang Z, Samanta A, *et al.* Autophagy inhibitor Lys05 has single-agent antitumor activity and reproduces the phenotype of a genetic autophagy deficiency. *Proc Natl Acad Sci USA* 2012; **109**:8253-8258.
72 Mullins MC, Nusslein-Volhard C. Mutational approaches to studying embryonic pattern formation in the zebrafish. *Curr Opin Genet Dev* 1993; **3**:648-654.
73 Kimmel CB, Ballard WW, Kimmel SR, Ullmann B, Schilling TF. Stages of embryonic development of the zebrafish. *Dev Dyn* 1995; **203**:253-310.
74 Knapik EW, Goodman A, Ekker M, *et al.* A microsatellite genetic linkage map for zebrafish (Danio rerio). *Nat Genet* 1998; **18**:338-343.
75 Shimoda N, Knapik EW, Ziniti J, *et al.* Zebrafish genetic map with 2000 microsatellite markers. *Genomics* 1999; **58**:219-232.
76 Thisse C, Thisse B. High-resolution *in situ* hybridization to whole-mount zebrafish embryos. *Nat Protoc* 2008; **3**:59-69.
77 Zhang Y, Bai XT, Zhu KY, *et al. In vivo* interstitial migration of primitive macrophages mediated by JNK-matrix metalloproteinase 13 signaling in response to acute injury. *J Immunol* 2008; **181**:2155-2164.
78 Wang L, Zhang Y, Zhou T, *et al.* Functional characterization of Lmo2-Cre transgenic zebrafish. *Dev Dyn* 2008; **237**:2139-2146.
79 Le Guyader D, Redd MJ, Colucci-Guyon E, *et al.* Origins and unconventional behavior of neutrophils in developing zebrafish. *Blood* 2008; **111**:132-141.
80 Link V, Shevchenko A, Heisenberg CP. Proteomics of early zebrafish embryos. *BMC Dev Biol* 2006; **6**:1.

(**Supplementary information** is linked to the online version of the paper on the *Cell Research* website.)

This work is licensed under the Creative Commons Attribution-NonCommercial-No Derivative Works 3.0 Unported License. To view a copy of this license, visit http://creativecommons.org/licenses/by-nc-nd/3.0